ZEUS - Note 01-004

Luminosity Measurement in the ZEUS Experiment

ZEUS Luminosity Group *

J.Andruszków, P.Borzemski†, J.Chwastowski, W.Daniluk,
A.Eskreys, P.Jurkiewicz, A.Kotarba, K.Oliwa, K.Olkiewicz,
M.B.Przybycień‡, W.Wierba, M.Zachara§, L.Zawiejski
Institute of Nuclear Physics, Cracow, Poland

L.Adamczyk, D.Kisielewska, M.Przybycień, L.Suszycki
Faculty of Physics and Nuclear Techniques,
University of Mining and Metallurgy, Cracow, Poland

January 25, 2001

Abstract

A precision luminosity measurement in the ZEUS experiment at HERA electron-proton collider is described. This description is based on the data collected by the ZEUS luminosity monitor in 1996. Method of the measurement relies on the detection of high-energy photons from *ep* bremsstrahlung process. The large cross section of this process allows for the continuous and fast monitoring of the HERA luminosity as well as for the control of the electron beam steering and focusing. A 1 % precision of the luminosity determination has been achieved. The ZEUS luminosity monitor has been also extensively used for studying at HERA quasi-real photoproduction events, and radiative processes in deep inelastic scattering.

*Supported within the DESY International Program and by the Polish Committee for Scientific Research, Grants: Nr 957/P03/97/12, Nr 115/E-343/SPUB/P03/120/96 and Nr 115/E-343/SPUB/P03/002/97

†Now at Computer Services Kaisha GmbH, Frankfurt Development Group
‡Now at Northwestern University, Evaston IL, USA
§Now at Qumak International Ltd., Cracow

Contents

1 Introduction **2**

2 Luminosity Monitor **5**

2.1 Detector Setup 5

2.2 Readout Electronics 7

2.3 Data Acquisition System 9

2.4 Performance of the Luminosity Monitor System 11

3 Background Processes **13**

3.1 egas Bremsstrahlung 14

3.2 Synchrotron Radiation 14

3.3 Proton Beam Halo and Other Background Processes 16

4 Luminosity Determination **17**

4.1 Correction for Event Pile-up 18

4.2 egas Background Subtraction 18

4.3 Correction for Geometrical Acceptance 18

4.4 Energy Scale Correction 21

5 Calculation of the Systematic Errors **24**

5.1 Event Pile-up 24

5.2 egas Background Subtraction 25

5.3 Acceptance Error 25

5.4 Theoretical Cross Section Uncertainty 26

5.5 Energy Scale Errors 27

5.6 Total Error 28

6 Summary and Outlook **29**

7 Acknowledgments **29**

1 Introduction

The collider luminosity $\mathcal{L}$ measures intensity of beam collisions and is defined by the relation:

$$R = \mathcal{L} \times \sigma, \tag{1}$$

where R is the event rate of process with the cross section σ. The standard unit of $\mathcal{L}$ is $\mathrm{cm}^{-2}\mathrm{s}^{-1}$. Value of luminosity depends on beam and collider parameters and can be either calculated provided a good knowledge of these parameters or can be measured using some well known process and Eq. 1. From the experimental point of view luminosity and beam energies are the most important parameters characterizing the collider performance.

HERA (Hadron Elektron Ring Anlage) is the collider type accelerator in which electrons are brought to the head-on collisions with protons, see Fig. 1. The particles in the HERA beams are grouped in bunches and these *bunches* cross the interaction point (IP) in 96 ns time intervals. Maximally 220 bunches can be stored in each of the HERA rings. To enable the direct determination of the beam related backgrounds the electron and proton bunches are grouped into "trains" having slightly different structure resulting in a number of non-colliding (i.e. without counter-rotating partners) *pilot* bunches, as shown in Fig. 2.

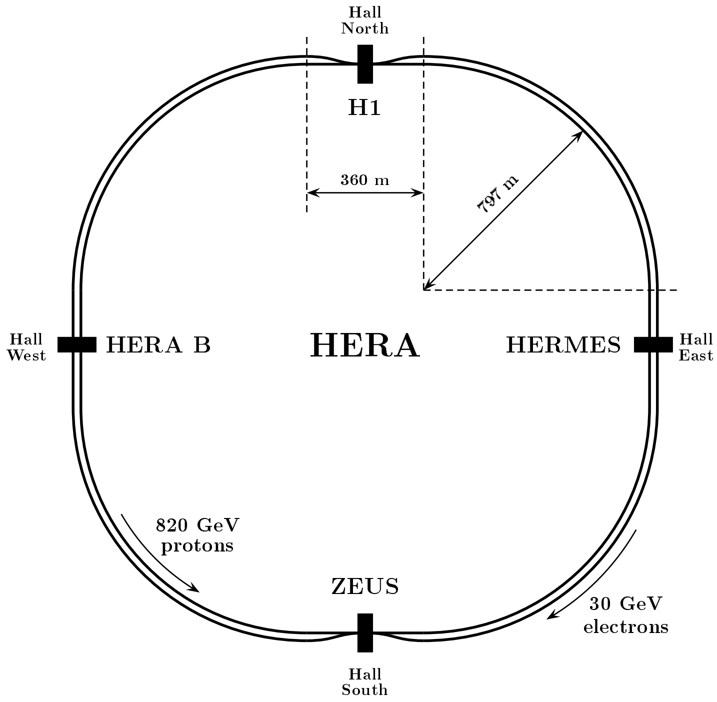

Figure 1: The general layout of the HERA collider.

In November 1991 HERA collider delivered 12 GeV electron and 480 GeV proton beams and the first *ep* collisions were observed by the luminosity monitors of the H1 and ZEUS [1] experiments. The experiments started taking data in late Spring 1992 with the

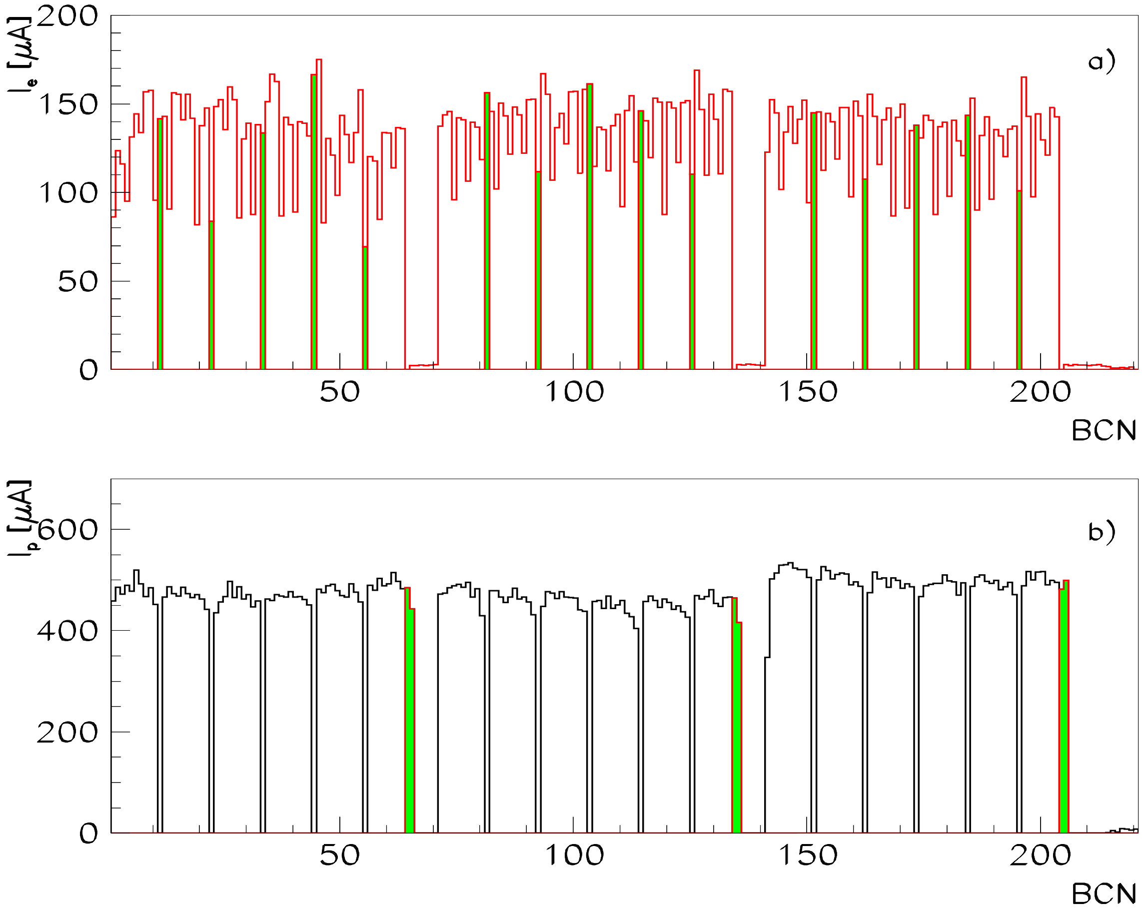

Figure 2: The distributions of the electron (a) and proton (b) bunch currents (in μA) in HERA. One histogram bin corresponds to a single bunch crossing number (BCN) and shaded bins represent pilot bunches.

beams of 26.7 GeV electrons and 820 GeV protons. The peak instantaneous luminosity was $1.7 \times 10^{29}\mathrm{cm}^{-2}\mathrm{s}^{-1}$ and integrated luminosity during 1992 was 30.6 nb^{-1}. Since then the collider performance has been gradually improved and in 1996 the delivered integrated luminosity was 17.2 pb^{-1} with the peak instantanous luminosity of 1.4×10^{31} $\mathrm{cm}^{-2}\mathrm{s}^{-1}$, very close to the design value. Between middle of 1994 and end of 1997 due to the problems with the electron beam lifetime at high beam currents, the electrons have been replaced by positrons[1]. To optimize the natural build up of the electron beam transverse polarization via Sokolov-Ternov process [2], the energy of the electron beam has been set to about 27.5 GeV since 1995. The luminosity measurement in the ZEUS experiment in its early phase has been described in our previous publications [1, 3, 4]. In the present article we describe the precision luminosity measurement as it was done in 1996.

[1]Through the article both positrons and electrons will be generically called electrons.

In order to measure luminosity using the Eq. 1 one chooses the process which has the cross section very well known from theory. The cross section should be large to allow for statistically precise measurement. To ensure good control of systematic uncertainties the process should have a clear experimental signature. Electron-proton bremsstrahlung process, $ep \to e'\gamma p$, fulfils these requirements and therefore was chosen for luminosity determination at HERA [3]. In this process the incoming electron radiates a high energy photon in the electromagnetic field of the proton charge. To a very good approximation the recoil of proton can be neglected and therefore the following relation is satisfied:

$$E_\gamma + E_{e'} = E_e, \tag{2}$$

where E_e is the electron beam energy, E_γ and $E_{e'}$ are energies of the radiated photon and scattered electron, respectively. The photon and electron spectra are described very well by the Bethe–Heitler formula [5] derived in the Born approximation neglecting spin and the finite size of the proton:

$$\frac{d\sigma_{BH}}{dE_\gamma} = 4\alpha r_e^2 \frac{E_{e'}}{E_\gamma E_e}\left(\frac{E_e}{E_{e'}} + \frac{E_{e'}}{E_e} - \frac{2}{3}\right)\left(\ln\frac{4E_p E_e E_{e'}}{M_p M_e E_\gamma} - \frac{1}{2}\right), \tag{3}$$

where α is the fine structure constant, E_p is the proton energy, M_p and M_e are the proton and electron masses, and r_e is the classical electron radius.

The bremsstrahlung photon and electron emerge from the IP at the very small angles Θ_γ, with respect to the incident electron direction. The angular distribution of the photons is described to a good approximation by the formula [6]:

$$d\sigma/d\Theta_\gamma \sim \Theta_\gamma/((M_e/E_e)^2 + \Theta_\gamma^2)^2. \tag{4}$$

The typical value of Θ_γ is of the order of M_e/E_e which corresponds at HERA to about 20 μrad. Since the horizontal (vertical) angular divergence of the electron beam at the IP is about 230 (70) μrad, therefore the photon angular distribution in the laboratory frame[2] is determined mainly by the angular spread of beam electrons.

The photon spectrum for low E_γ is suppressed due to small lateral dimensions of the colliding beams [7]. This so called beam size effect occurs because of extremely small momenta transfers involved (even less than 0.01 eV) in the high energy bremsstrahlung process [8].

Initially, the luminosity was measured [1] by detecting in coincidence a high energy photon and a scattered electron which satisfied within experimental uncertainties Eq. 2. However, already in 1992, because of very good background conditions as well as a high and well controlled photon acceptance, it was decided to use only photons for the precise luminosity determination. Hence, the luminosity measurement is based on counting the rate of high energy bremsstrahlung photons. The measurement of the scattered electrons has been still used for the systematic checks.

The luminosity monitor also detects photons radiated by an electron prior to (initial state radiation–ISR) or after (final state radiation) interaction with a proton. ISR effectively lowers the center-of-mass energy of the ep collision and allows for extension of the

[2]The ZEUS coordinate system is defined as right-handed with the Z axis pointing in the proton beam direction, and the X axis in the horizontal plane, pointing towards the center of HERA.

kinematical range of the proton structure studies at HERA. The luminosity monitor has been used in the measurement of F_2 structure function [9], and can possibly be used for extraction of the longitudinal structure function F_L [10].

The electron measured in the luminosity monitor (in absence of the photon) has been used to 'tag' the photoproduction events at HERA [11, 12, 13]. It has also been used for important systematic check of the energy scale in reconstruction of the photoproduction events and the estimation of the photoproduction background corrections in the deep inelastic scattering (DIS) studies.

2 Luminosity Monitor

Since the emission angles of bremsstrahlung photons and electrons are small (of the order of M_e/E_e for photons and $M_e/E_{e'}$ for electrons [6]) both electron and photon travel initially inside the HERA beam pipes. Two technical aspects of the HERA construction turned out to be essential in the design and construction of the luminosity monitor:

- at about 80 m from the IP the proton beam is bent upwards and only beyond this area the photons can leave the proton beam pipe;
- the bremsstrahlung electrons have energy lower than the beam energy. The electron beam-line magnets, adjacent to the straight section which surrounds the IP, act as a spectrometer, bending more the off-beam energy electrons towards the center of the ring. These electrons at some distance from the IP can leave the electron beam pipe and be detected.

The exit windows at the beam pipes could be conveniently installed at $Z = -7.8, -27.3$ and -43.6 m for electrons and at $Z = -92.5$ m for photons. At these distances the detectors have to be placed inside the HERA tunnel, close to the electron beam pipe (the electron detectors) and to the proton beam pipe (the photon detector). The optimal positions which match the configuration of the HERA beam-line elements were found at $Z = -8, -35$ and -44 m for the electron detectors and $Z = -107$ m for the photon detector. Fig. 3 shows the general layout of the luminosity monitor detectors with respect to the HERA beam-lines.

2.1 Detector Setup

The photon detector consists of:

- a copper-beryllium window 0.095 X_0 ($X_0 \equiv$ radiation length) thick at $Z = -92.5$ m;
- followed by a 12.7 m long vacuum pipe;
- followed by an absorber (*filter*) which shields against a large flux of direct synchrotron radiation, made of a 2 X_0 thick graphite block;

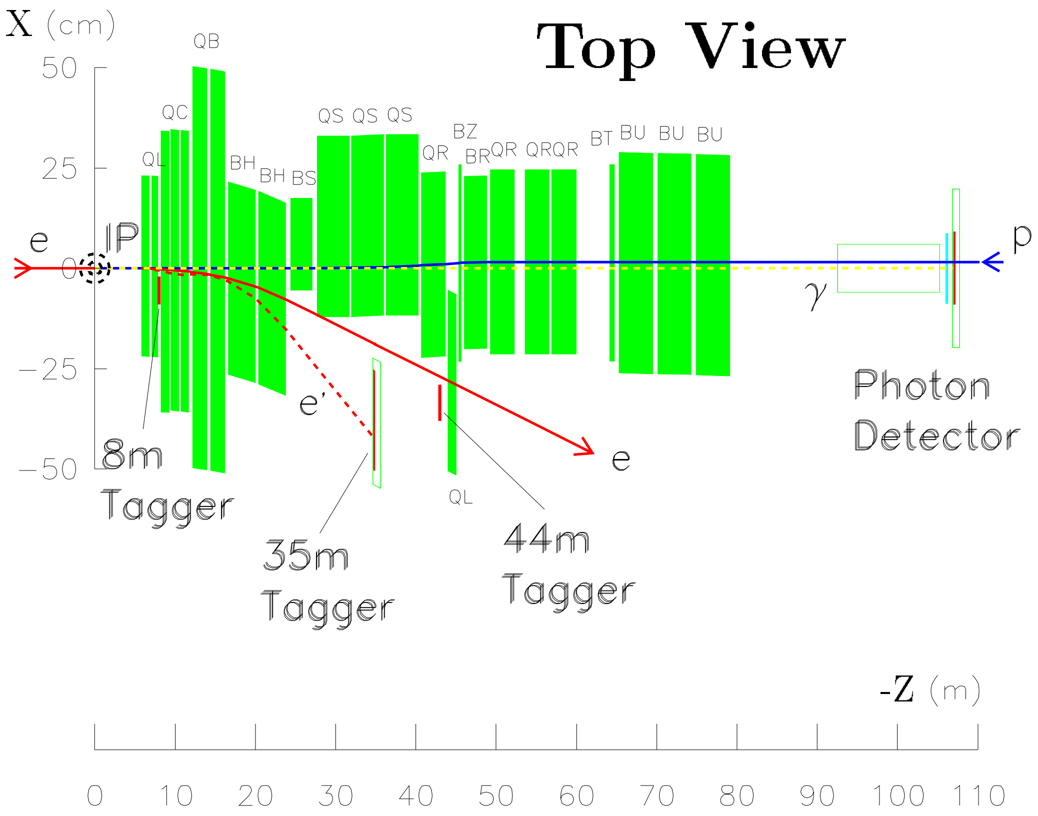

Figure 3: General layout of the ZEUS luminosity monitor. Note very different scales used for Z and X dimensions.

- followed by the lead–scintillator sampling calorimeter with a detector measuring shower position, inserted at the depth of 3 X_0. The sampling is done in 1 X_0 steps but the nominal thickness of the scintillator layers of 2.6 mm is changed in front part of the calorimeter (before the position detector) in order to compensate energy losses in the absorber, see Fig. 4. The scintillator plates made of SCSN-38 are optically coupled through a thin air gap to top and bottom wave-length shifter (WLS) plates. To one edge of WLS plate a plastic bar is glued and guides the light to a photomultiplier tube (PMT). The calorimeter has transversal dimensions of 18 cm$\times$18 cm and the depth of 22 X_0. From sides it is shielded against the non-direct synchrotron radiation by 1 cm thick lead plates. The calorimeter is installed on a movable table, and during beam injection and acceleration is remotely parked away behind shielding made of the lead bricks.

The position detector consists of two layers of 1 cm wide scitillator strips which are read from one end by P-I-N photodiodes, one set of strips is oriented horizontally and is used for measurement of the vertical position, the other set is oriented vertically and is used for measurement of the horizontal position [14].

The detector measures efficiently photons with energies larger than a fraction of GeV emerging from the IP at angles with respect to the $-Z$ axis smaller than approximately 0.5 mrad. The relative energy resolution is about $20\%/\sqrt{E(GeV)}$, and the spatial resolution of the position detector is of the order of 3 mm [14] corresponding to the uncertainty of the reconstructed photon angle of about 30 μrad.

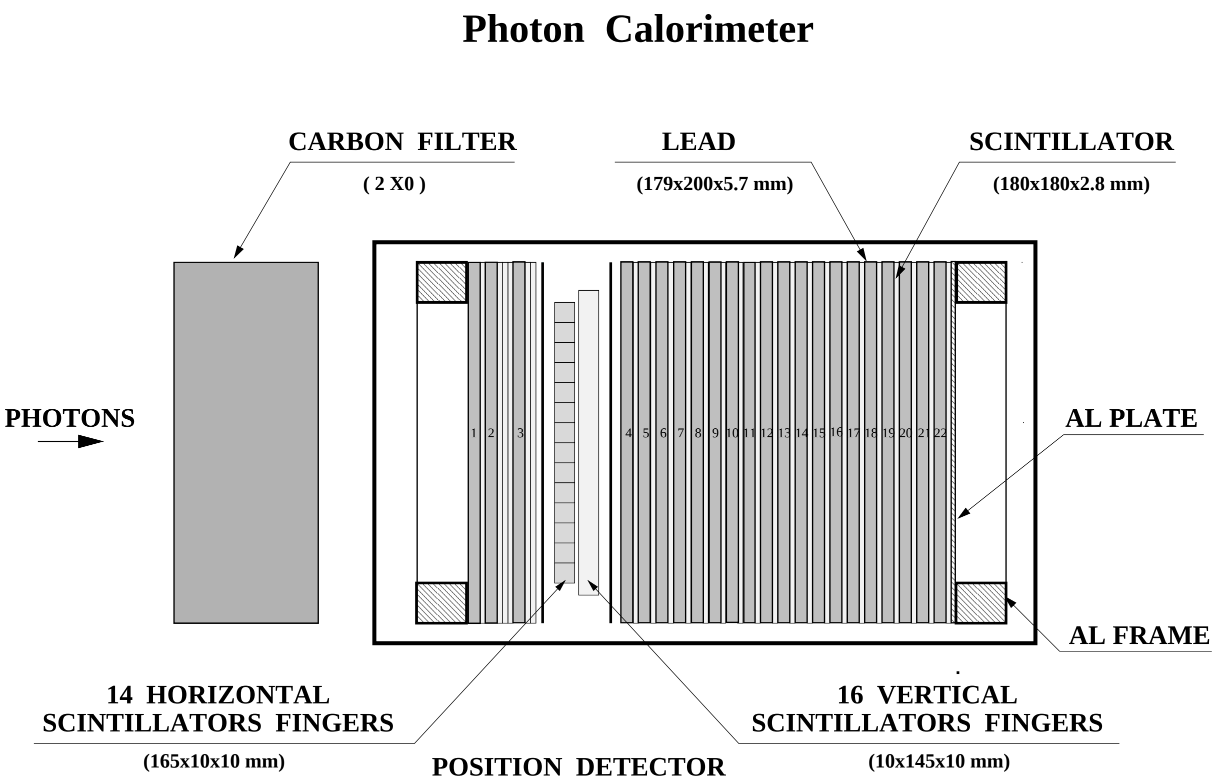

Figure 4: Schematic side view of the photon detector in the 1996 configuration.

The electron detector located at $Z = -35$ m, behind a $0.085X_0$ thick steel exit window, has construction very similar to that of photon detector. It is a 22 X_0 deep lead–scintillator sampling calorimeter with the electron position detector inserted at the depth of 7 X_0. The sampling step is 1 X_0 and is uniform throughout the calorimeter. The transversal dimensions of the calorimeter are 25 cm$\times$25 cm. The energy of the electrons reaching the detector is in the 5–21 GeV range.

The electron detectors located at $Z = -8$ and -44 m [13] are small tungsten-scintillator sampling calorimeters with the scintillator strips or fibers used for reconstruction of the horizontal position of the electromagnetic showers. The average energies of the electrons reaching these detectors are about 2 and 24 GeV, respectively.

In the following, only the photon detector and the electron detector located at $Z = -35$ m are discussed.

2.2 Readout Electronics

The block diagram of the front-end electronics for two energy channels of the photon detector is presented in Fig. 5. The 12-dynode photomultiplier tubes, Hamamatsu R580, are powered by resistor voltage-dividers. To minimize PMT gain drifts due to large event rates, resulting in large currents flowing between the last dynodes, the voltage-dividers are very progressive. Division ratio of 27 is used and the last two dynodes are powered separately. This solution ensured good gain stability at 1–2 % level for average anode currents below 10 μA, and at 3–4 % level at 20 μA. The photomultiplier anodes are terminated with 100 Ω resistors and are directly coupled to the voltage amplifiers with a 10-fold gain (VV100B LeCroy). The output signal is fed via 20 meters coaxial cable to the analog readout electronics which is placed in the electronics rack under the floor of the HERA tunnel. Auxiallary output signals of the amplifiers were fed via 200 m long lines used for the remote testing and monitoring purposes.

The analog readout electronics consists of input amplifiers followed by the fast custom-made integrators. The integrators are based on fast voltage-to-current converters coupled to integrating capacitors, and work with a 65 ns gate and require about 30 ns for full discharge. The integrators are directly coupled to 8–bit flash analog-to-digital converters (FADC's).

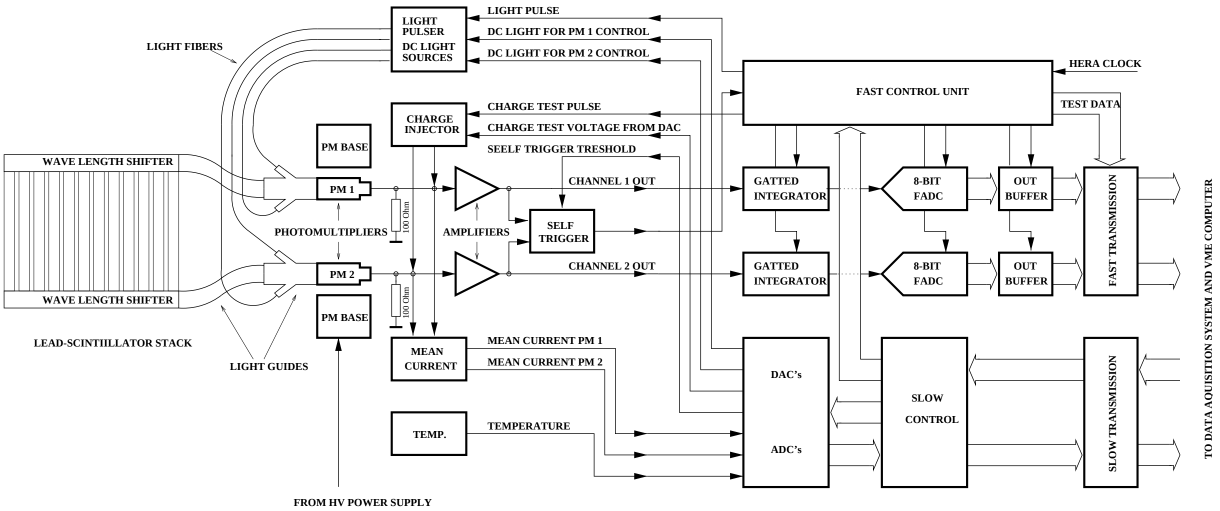

Figure 5: Block diagram of the readout electronics (energy channels).

The precision light pulsers are installed in each calorimeter for monitoring of the overall gain of the analog electronics. Capacitors with low temperature drifts are charged using 12-bit digital-to-analog converters (DAC's). For good stability the circuits are installed in the thermostatic chambers. The capacitors are discharged by light-emitting diodes (LED's) producing stable and fast (with about 12 ns decay-time) light pulses. LED's are optically coupled to the PMT plastic bars described above.

There are two independent methods used to measure the average PMT anode currents. The first method is based on RC integrators with 2 ms time constants. In the second method, the currents floating into the last and last-but-one dynodes of a PMT are measured at the HV power supply unit. Using the dynode multiplication factors the anode currents can be derived .

The precision charge injectors with 12-bit resolution are also used for testing linearity and stability of the electronics chain excluding PMT's. In particular, it allows for *in situ* measurement of FADC differential non-linearities.

Temperature inside the calorimeter housing is monitored continuously. The typical temperatures are in the 30–40 ^{0}C range, varying with the day-night cycle and with the actual status of the HERA system.

The position detector front-end electronics is described in [14]. The position detector analog signals are digitized in a similar manner as for the calorimeter channels.

2.3 Data Acquisition System

The luminosity monitor data acquisition (DAQ) system is based on the custom-made electronics boards using the VME–bus and the standard ZEUS transputer boards [15].

The digital data stored in the electronic racks in the HERA tunnel are transferred at 10.4 MHz frequency of HERA bunch-crossings to the electronic racks situated in the ZEUS experimental hall in a hut called *rucksack*. The digital signals are sent differentially, for over about 130 and 200 m long twisted-pair cables for the electron and photon branches respectively. The parity-bit is checked for each 16-bit block of the transmitted data.

The received data are stored in the following hardware buffers (see Fig. 6):

- the *raw data buffer* stores raw ADC counts from four (two photon and two electron) photomultipliers. This circular buffer is continously being filled with frequency of 10.4 MHz and has capacity of storing the data from one revolution of HERA beams (220 events);
- the *calibrated data buffer* stores 8-bit average ADC counts, obtained for each calorimeter by a hard-wired calibrator which works as a look-up-table, and a 8-bit event type flag set by the *lumi-processor*. This circular buffer has also capacity of storing 220 events;
- the *position data buffer* stores the data transferred on request from the electron and photon position detectors. This data corresponds to events with a particular flag in the *calibrated data buffer*. It has capacity of 256 events.

The lumi-processor board sets flags for various types of events as bremsstrahlung, photoproduction or radiative photon event candidate. It contains also scalers counting without dead-time bremsstrahlung events separately for bunch crossings with the colliding and electron pilot bunches.

On-line calculation of the luminosity and reconstruction of the hit position in both position detectors is made on a dedicated workstation. For the data presentation and data monitoring the two X-windows applications were developed:

- the histograms presenter which allows quick and easy validation of the data collected by the luminosity detectors;

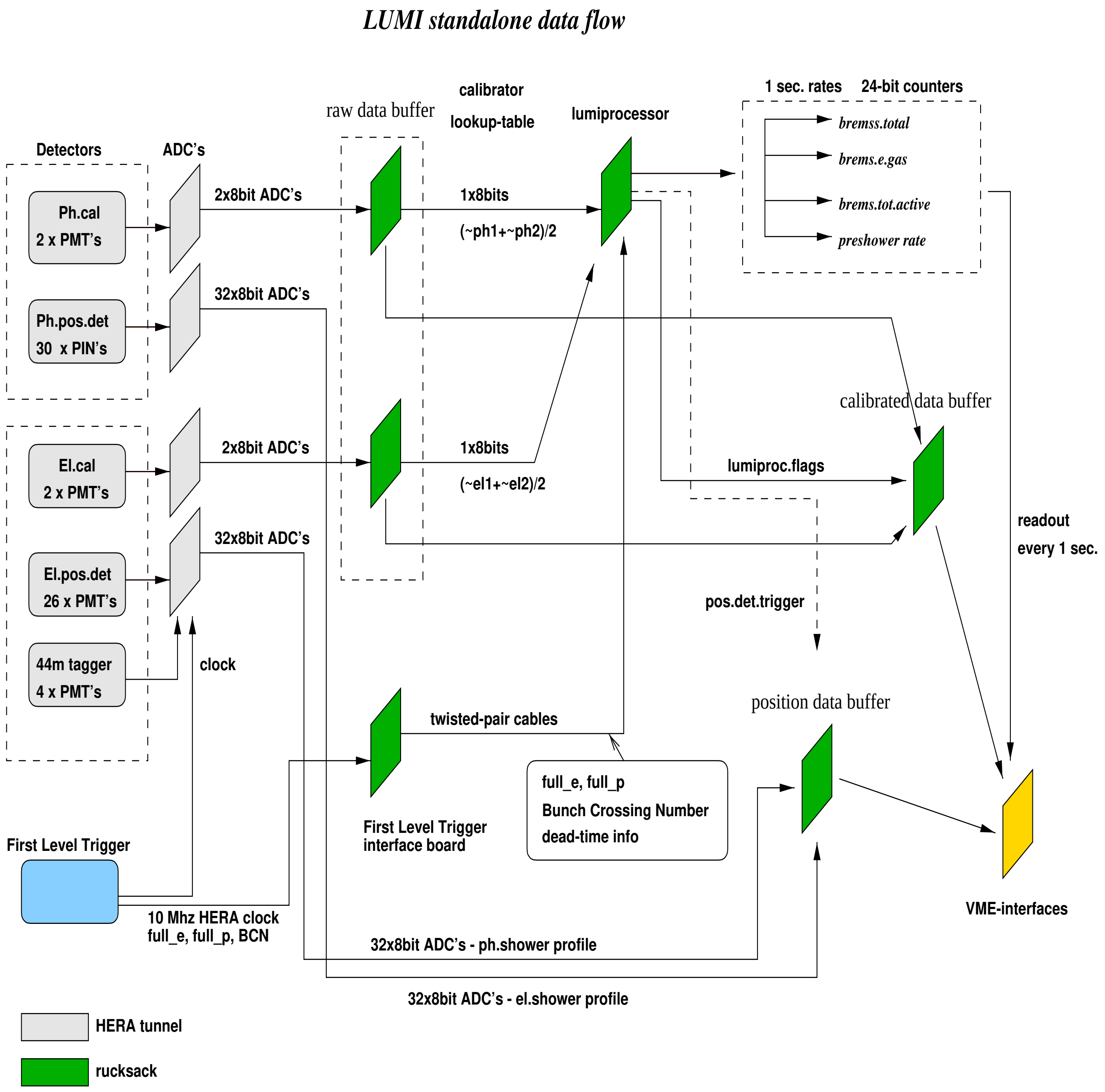

Figure 6: Diagram of the stand-alone data flow of the luminosity detector DAQ system. Darker shaded components are placed in the rucksack, the rest is in the tunnel

- the display of the on-line event rates, short-term (one entry per second) and long-term (one entry per several minutes) history of the HERA luminosity, the measured electron beam angular distribution and its history, and other on-line information relevant for monitoring the detector performance.

The results of the luminosity calculation are distributed to the ZEUS experiment by the server which uses the special ZEUS network protocol. The work of the luminosity monitor is controlled by the ZEUS shift crew with a run-control process, but it can be also activated independently.

The diagram shown in Fig. 6 describes the data flow of the luminosity monitor system which also delivers data to the three level trigger system of the ZEUS experiment [15]. At the first level trigger (FLT) stage the raw data from photon and electron calorimeters are used. In addition, a large set of the FLT scalers is used to count the various types of bremsstrahlung events, e.g for selected HERA bunch crossings. The communications with the higher trigger levels and the ZEUS event builder [15] is done using the transputer board. Additionally, every approximately 14 seconds a part of the data from the internal buffers is stored in the ZEUS so-called *environmental records*. This data is used for the off-line luminosity calculation and serves also for monitoring and calibration purposes. The luminosity DAQ system has been working reliably and is capable to run dead-time free with the design 1 kHz output rate to the FLT, and with the maximum latency of delivering the data to the FLT of 2 μs.

A slow control system is used to set running conditions of the luminosity monitor as the HV settings, modes of the data taking, the detector configuration, for example. It also monitors some parameters as the detector temperatures and the PMT anode currents, and communicates the general status of the luminosity monitor to the central ZEUS slow control system.

2.4 Performance of the Luminosity Monitor System

The light from the scintillator layers is collected on the top (up) and bottom (down) side of the photon calorimeter and is transported through the light guides and WLS and read out by two PMT's. From the two ADC values ADC_{up} and ADC_{down} the arithmetical average ADC_γ corrected for pedestals is calculated:

$$ADC_\gamma = (ADC_{up} + ADC_{down})/2 - (ADC^{ped}_{up} + ADC^{ped}_{down})/2 \tag{5}$$

where ADC values are rounded to the integer values. ADC^{ped}_{up} and ADC^{ped}_{down} are the ADC pedestal values for the two PMT's.

For monitoring two ADC pedestals which correspond to the top and bottom WLS readouts of the photon calorimeter (right and left ones for the electron calorimeter), distributions of the ADC counts are measured continuously using the random trigger data, as shown in Fig. 7a,c. The width of the distributions is due to the noise in electronics and corresponds to the photon energy of about 50 MeV. The pedestals ADC^{ped}_{up} and ADC^{ped}_{down} are defined as the average of these distributions. Fig. 7b,d shows typical pedestal variations during one long run.

In Fig. 8 the measured pedestals are plotted as a function of the bunch crossing number. The observed structure in this figure can be attributed to the three interplaying effects:

- for full electron bunches the synchrotron radiation shifts the pedestals up;
- for the empty electron bunches there is no contribution from the synchrotron radiation and

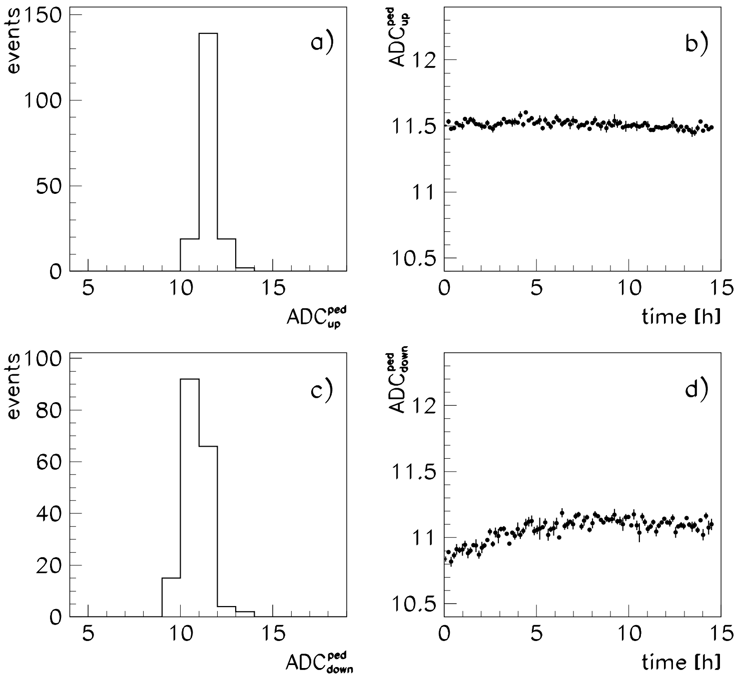

Figure 7: Distributions of the photon calorimeter ADC counts in upper (a) and lower (c) phototubes for random triggers; (b,d) time dependence of the measured ADC pedestals in upper and lower PMT's for a single long run.

- a kind of pile-up effects between neighbouring electron bunches are present.

The shift does not fluctuate significantly for a given electron bunch. It however slowly decreases as a consequence of the decreasing electron beam current. Only rarely it can change quickly due to re-steering of the electron beam which may result in a significant change of the electron orbit inside the quadrupoles, hence affecting the intensity of synchrotron radiation.

Variation of overall gain of the analog electronics is monitored continously with a 0.1% statistical precision each few minutes using the LED pulser data, see Fig. 9. The gain decreases during the first hours of running typically by 1% due to relatively fast decrease of the event rate, resulting in a significant decrease of the PMT anode current. To monitor the overall energy scale as well as the background conditions distributions of the average ADC counts ADC_γ for photon energy above ≈ 0.5 GeV are stored at the rate of about 10^6 entries/minute for the colliding bunches (Fig. 10 a) and at the rate of about 10^4 entries/minute for the electron pilot bunches (Fig. 10 b). The spike visible at the end of distribution in Fig. 10 a is due to overflows.

The distributions of the sum of the photon and electron signals are also stored to control the electron detector energy scale and the energy resolution of the two calorimeters, see Fig. 11.

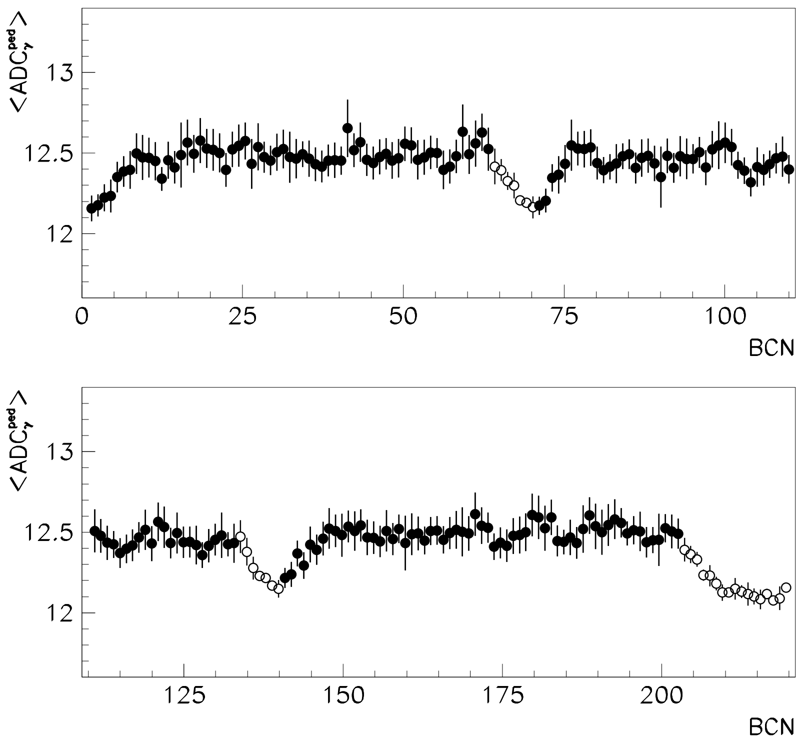

Figure 8: The measured pedestals (averaged from the two phototubes of the photon calorimeter) are plotted as function of the bunch crossing number. The data corresponding to filled electron bunches is marked as full circles, whereas the data for empty electron bunches are marked as open circles.

The spatial distributions of the incoming particles in the photon and electron detectors are also continuously monitored using the data from the position detectors. The average lateral photon position is determined every few seconds with a statistical precision better than 0.5 mm corresponding to a 5 μrad angular uncertainty.

The major irradiation of the detectors is caused by the energy depositions due to the bremsstrahlung events. In the photon detector the annual dosage in the area close to the maximum development of the electromagnetic showers is about 1000 Gray. The expected loss of the light yield in SCSN–38 scintillator for this dosage is about 2% [**?**].

3 Background Processes

The background processes can fake the ep bremsstrahlung signal or, may also deteriorate performance of the luminosity monitor. The most significant background is due to the process of the electron bremsstrahlung on the residual gas molecules inside straight section of the beam pipe close to the IP. The background due to synchrotron radiation of the electron beam effectively shifts the observed ADC pedestals. The proton beam related backgrounds are not significant, except for precision studies of the low energy deposits in the photon detector.

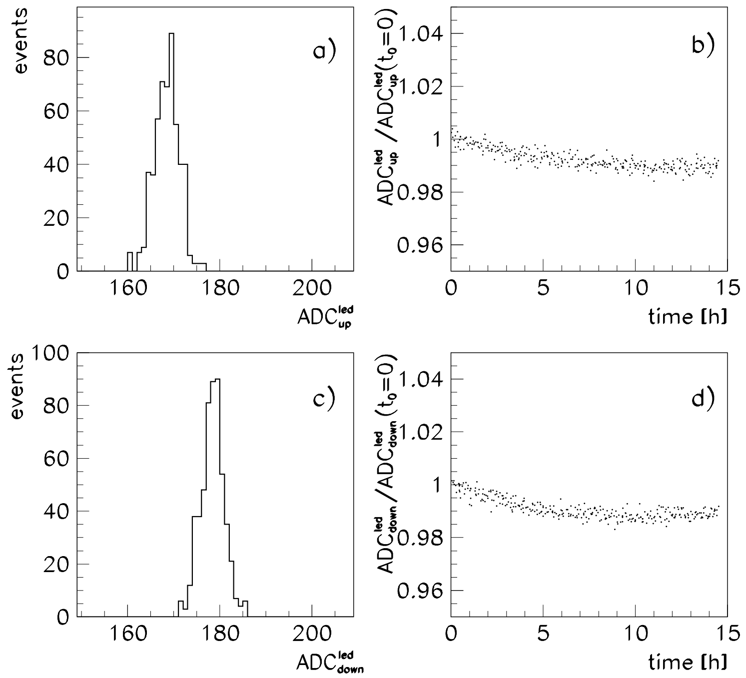

Figure 9: Distributions of the ADC counts for the LED pulser data in upper (a) and lower (c) PMT's; the time dependence of the average signal normalized to initial values for a single long run in upper and lower PMT's (b,d).

3.1 egas Bremsstrahlung

The electron-gas (*egas*) bremsstrahlung, $eZ \to e'\gamma Z$, has practically the same signature as the *ep* bremsstrahlung, and its contribution can only be estimated statistically. This is done using the electron pilot bunches as described in Sec. 4.2. The *egas* events observed in the photon detector originate from interactions of beam electrons with the residual gas in the region -6 m $< Z <$ 6 m. The rate of *egas* bremsstrahlung is proportional to the electron beam current and is also proportional to the measured gas pressures as can be seen in Fig. 12.

The residual gas pressure is measured by the gauges located at about $Z = \pm 5.5$ m and is typically of the order of 10^{-10} mbar. During one beam store it typically varies by a factor of 3–4, see Fig. 12.

3.2 Synchrotron Radiation

The main source of the synchrotron radiation is the electron beam bent in the horizontal plane inside the quadrupole magnets closest to the IP at about $Z = \pm 6$ m. Only the photon detector is exposed to the direct synchrotron radiation. For the nominal electron orbit the bending radius should be 1360 m. However dedicated studies indicated somewhat

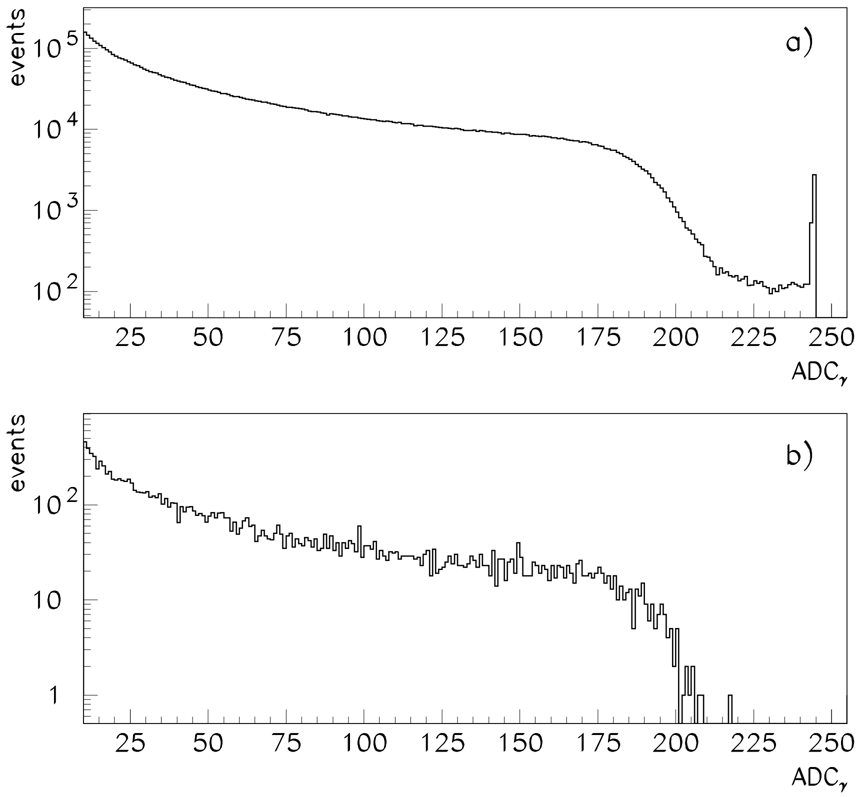

Figure 10: Distributions of ADC_γ for the colliding bunches (a) and for electron pilot bunches (b).

smaller value for the typical running conditions [16]. The radiated power inside the cone in the photon detector geometrical acceptance is of the order of 100 W. This requires a water cooling of the copper-beryllium photon exit window which absorbs its significant fraction.

The direct radiation is attenuated by the absorber in front of the photon calorimeter. Additionally, the detectors are shielded from all sides against the scattered synchrotron radiation filling the whole volume of the HERA tunnel. However, at the same time the absorber deteriorates the photon energy measurement and therefore its thickness and composition has to be optimized. Low energy part of the synchrotron radiation is very efficiently absorbed by copper in the photon exit window and lead in the calorimeter plates. The high energy part is very penetrating and requires use of light materials. The remaining radiation after attenuation in the carbon absorber leads effectively to the shifts of the ADC pedestals by ≤ 0.4 ADC counts corresponding to ≤ 50 MeV energy deposition (see section 2.4).

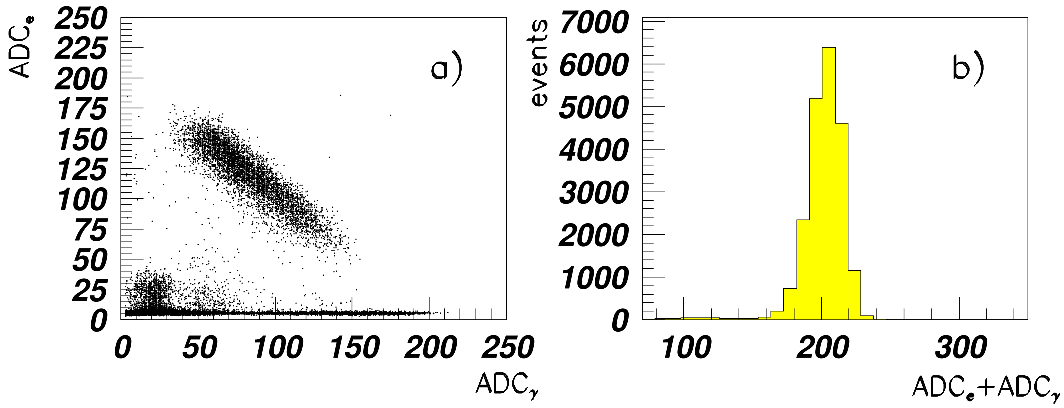

Figure 11: Correlation plot of the electron $ADC_{e'}$ and photon ADC_γ (a) and the distribution of the sum $(ADC_{e'} + ADC_\gamma)$ (b).

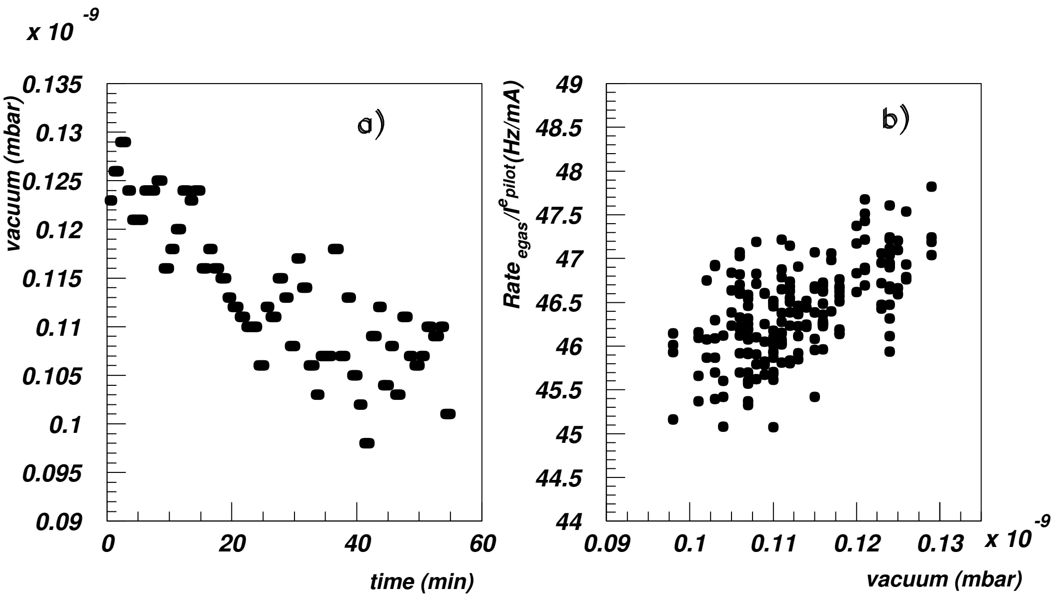

Figure 12: (a) Time dependence of the residual gas pressure measured by a gauge at $Z = -5.5$ m in a single ZEUS run; (b) the correlation between the measured pressure and the bremsstrahlung rate for electron pilot bunches, $Rate_{egas}$, normalized by the corresponding current of the pilot bunches, I^e_{pilot}.

3.3 Proton Beam Halo and Other Background Processes

Particles traveling with the proton bunches (proton beam halo) as well as the secondaries produced by their interactions with the HERA proton beam elements can hit the luminosity monitor detectors and lead to additional energy depositions. To minimize this effect the photon detector is installed at a position where at the moment when a bremsstrahlung photon reaches it, the two closest proton bunches are 14 m before and 14 m after the photon detector [17]. However, the background signal can be still observed due to a finite detector response time. This background was initially significant [1] but after improving the proton beam lifetime it became negligible.

The back-scattering of the thermal photons on the beam electrons in the Compton process [8], leads to enhancement in the measured photon spectra below 2–3 GeV as can be seen in Fig. 17. Other processes like the two-photon production of e^+e^- pairs in ep interactions have negligible rates [16].

4 Luminosity Determination

To calculate luminosity Eq. 1 is used:

$$\mathcal{L} = R^{ep}/\sigma_{BH}^{obs}, \tag{6}$$

where R^{ep} is the measured rate of ep bremsstrahlung events and σ_{BH}^{obs} is the bremsstrahlung cross section calculated for the given selection cuts and corrected for the detector effects and the geometrical acceptance of bremsstrahlung photons.

The bremsstrahlung events are selected in several ways, i.e. by requiring signals in the photon calorimeter to be above threshold values of about 2, 5 and 10 GeV or, within 10–16 GeV energy range. These different types of event selection (in further called also triggers) were done to maximize control of systematic uncertainties due to the selection procedure.

High event rates, typically in 100 kHz to 1 MHz range for $E_\gamma > 2$ GeV, correspond to up to 10% probability of detecting an event in a given bunch crossing. It results in a significant event pile-up, i.e. occurence of two or more bremsstrahlung photons in the same bunch crossing. Since such multiple events are not resolved the counting of events is affected and requires a correction for this effect. The subtraction of the $egas$ bremsstrahlung contribution is done using the directly measured $egas$ event rates from the electron pilot bunches.

The photon acceptance is purely geometrical, i.e. does not depend on the photon energy. Therefore σ_{BH}^{obs} can be factorized :

$$\sigma_{BH}^{obs} = A_\gamma \sigma_{BH}^{corr}. \tag{7}$$

The acceptance A_γ is calculated using a Monte Carlo program which simulates the relevant beam line apertures and is tuned to describe the measured photon angular distributions. Finally, the cross section σ_{BH}^{corr} is calculated using the Monte Carlo event generator BREMGE [18] which simulates the ep and $egas$ bremsstrahlung processes in Bethe-Heitler approximation, as well as the beam size effect according to the theoretical estimates [8]. The detector effects are parametrized in a simple form [7] and the event selection is then done exactly as in the real experiment.

All these steps in the luminosity determination are discussed in more detail in the following sections.

4.1 Correction for Event Pile-up

The event pile-up may increase or decrease the event counting rates. In the first case the additional events are counted because two or more concurrent bremsstrahlung photons which individually would fail the selection cuts, together satisfy the cuts. In the second case, less events is counted for example when two 'good' bremsstrahlung photons are counted as a single event. The Monte Carlo simulation [7] shows that counting of the events with energy deposition above $\approx$ 5 GeV (5 GeV trigger) is least sensitive to the event pile-up i.e for this trigger the event losses balance the gains. Experimentally, the counting rates for the colliding bunches are corrected for event pile-up using the formula:

$$R^{coll} = \tilde{R}^{coll}(1 + a\tilde{R}^{coll}/N_{coll}) \tag{8}$$

where R^{coll} is the corrected rate, $\tilde{R}^{coll}$ is the corresponding uncorrected rate, N_{coll} is the total number of the colliding electron bunches and a is the coefficient obtained from the Monte Carlo simulation. This procedure assumes that the event rates are not too high and mainly double events contribute to the event pile-up. Eq. 8 is applied for each trigger separately assuming the typical relative contributions of the ep and $egas$ brewmsstrahlungs (see the next subsection). The pile-up effects for the electron pilot bunches are neglected since their rates are about 30 times smaller than for the colliding bunches. The correction procedure also assumes that bunch-to-bunch rate variations are not large.

4.2 egas Background Subtraction

The electron-proton bremsstrahlung rate R^{ep} is calculated from the formula:

$$R^{ep} = R^{coll} - kR^{pilot} \tag{9}$$

where R^{pilot} is the $egas$ event rate measured using the electron pilot bunches and the factor $k = I_e^{coll}/I_e^{pilot}$ is the ratio of the total electron current for the colliding bunches to that in the pilot bunches. The procedure assumes that the contribution from $egas$ events scales with the electron current. In particular, it assumes the same bunch-to-bunch pressure of the residual gas and the geometrical properties of the electron beam as e.g. the tilt or angular divergence. Typically, $egas$ contribution is at 3 % level.

4.3 Correction for Geometrical Acceptance

According to a detailed simulation of the HERA beam line using the GEANT program [19] the electromagnetic showers induced by the high energy photons hitting some obstacle upstream of the photon detector do not deposit significant energy in the photon calorimeter. It means that the efficiency of the photon detection can be factorized into a geometrical acceptance ($\equiv$ probability of reaching the photon calorimeter) which does not depend on the photon energy and the response function of the photon calorimeter.

The geometrical acceptance depends on:

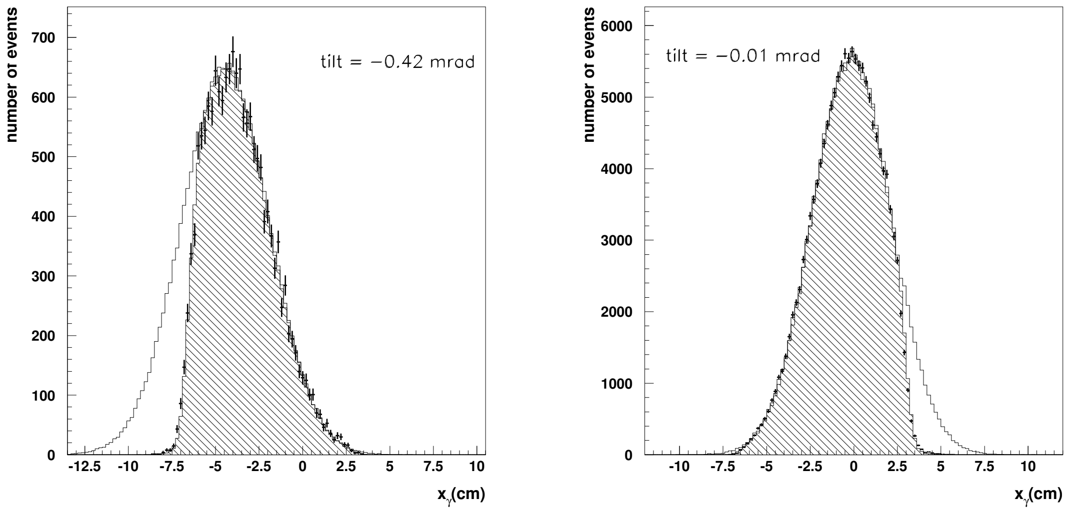

Figure 13: Distributions of the measured (points) and simulated (hatched histograms) bremsstrahlung photon positions for runs with large electron beam tilts. The Monte Carlo distributons assuming no absorption of photons in the HERA beam line are overlaid (open histogram).

- the inner apertures of the HERA beam line which define an 'obstacle-free' path of bremsstrahlung photons;
- the geometrical properties of the electron beam at the IP, in particular the electron beam tilt and its angular divergence.

The contour of the most limiting apertures is experimentally determined using the photon position data from dedicated runs with the extreme electron beam tilts when the apertures significantly obscure the path of bremsstrahlung photons. A simple Monte Carlo model is used to simulate in three steps the photon position measurement:

1. Generating of the photon angular distribution according to the electron beam angular divergence and the bremsstrahlung emission angles.
2. Rejecting photons with angles outside the cone defined by the acceptance contour.
3. Smearing of the photon position at $Z = -107$ m according to the spatial resolution of the position detector.

The shape of the acceptance contour is changed in the Monte Carlo simulation until the best description of the position data is achieved, see Fig. 13. The acceptance contour found in this way and the distribution of bremsstrahlung photons projected on the face of the photon detector are shown in Fig. 14. The acceptance A_γ is then equal to the fraction of photons in the Monte Carlo simulation which reached the photon detector

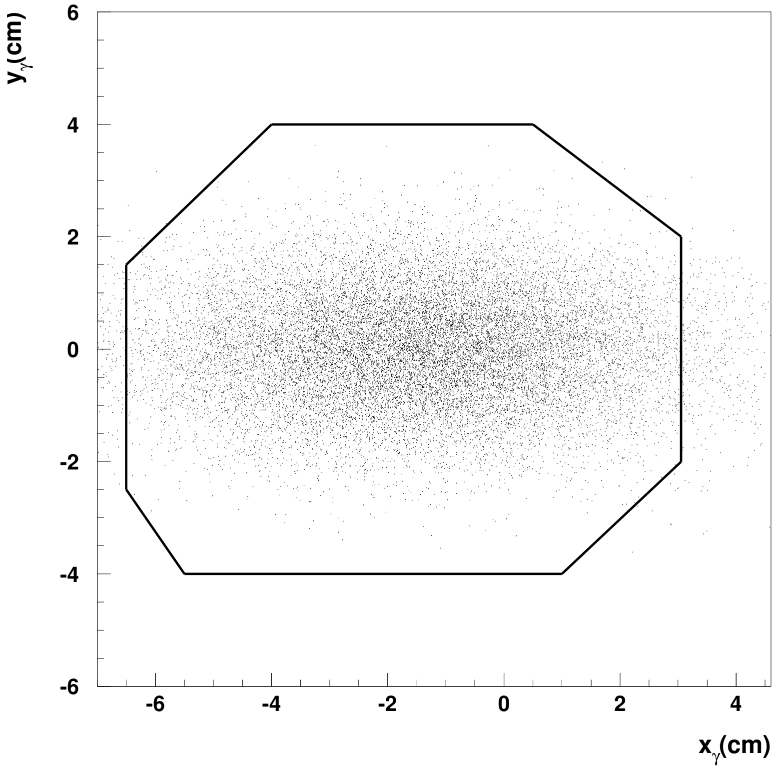

Figure 14: Projection of the acceptance contour (solid lines) and 'true' spatial distribution (points) of the bremsstrahlung photons on the face of the photon detector.

(= fraction of events inside the contour), see Fig. 14. The acceptance is calculated for different horizontal tilts of the electron beam and for different horizontal angular divergences, see Fig. 15. Because of the small vertical angular spread, the variation of the photon acceptance due to the relatively small vertical tilts of the electron beam could be neglected.

The acceptance A_γ is tabulated as a function of the average position and the width of the bremsstrahlung photons beam measured by the position detector and is continuously updated for the luminosity determination. For the nominal horizontal tilt of the electron beam of -150 μrad (no vertical tilt) and for the horizontal and vertical angular beam divergences of 230 and 70 μrad, respectively, the geometrical acceptance is almost 98%. For the off-line luminosity calculation the average and the dispersion of the photon position is determined with the high statistical precision every three minutes of the ZEUS run. The appropiate correction is then applied.

The determination of the photon acceptance in only one way described above may be considered as shortcoming of the whole procedure of luminosity determination. The only other independent way, based on the electron detection was investigated. As the photon acceptance is independent of the photon energy for the process of bresstrahlung (the angle of the bremsstrahlung photon emission is practically 0^o independently of the photon energy) it should be possible to choose such an energy interval for electrons for which their acceptance in the electron calorimeter is high and energy independent.

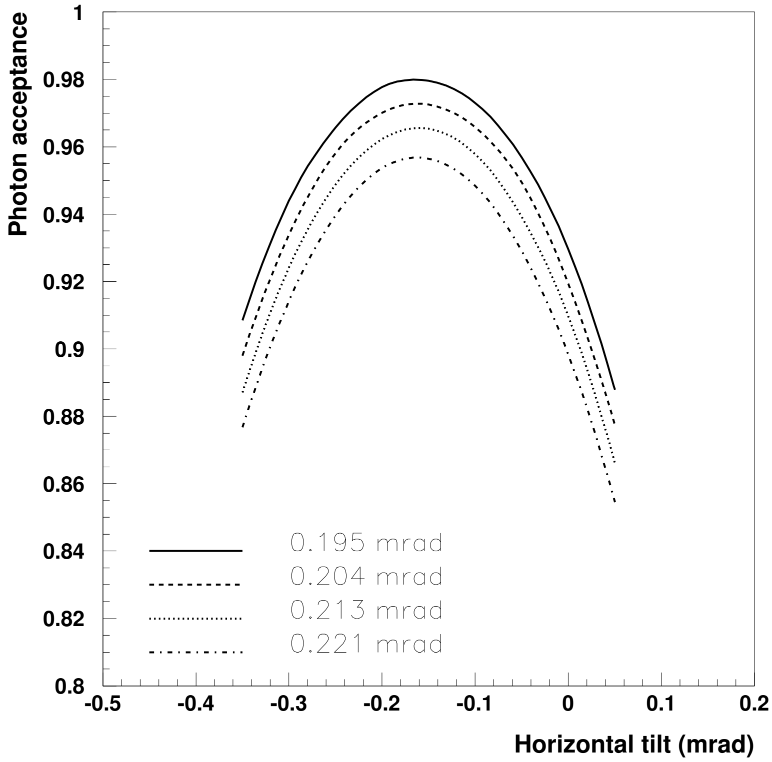

Figure 15: Geometrical acceptance of the photon detector A_γ for several values of the electron beam horizontal divergence as a function of the horizontal electron beam tilt.

Then, in an ideal situation one could determine the photon acceptance by measuring the ratio of the number of electrons associated with the detected photon to all detected electrons in this energy interval. The photon acceptance calculated this way may be expressed as:

$$A_\gamma^* = \frac{\int\int [F(x_\gamma, y_\gamma) \cdot A_{el}(\Delta E_{el}) \cdot A_\gamma(x_\gamma, y_\gamma)] dx_\gamma dy_\gamma}{\int\int [F(x_\gamma, y_\gamma) \cdot A_{el}(\Delta E_{el})] dx_\gamma dy_\gamma}, \tag{10}$$

where $A_{el}(\Delta E_{el})$ is the electron acceptance in the energy interval ΔE_{el}, $A_\gamma(x_\gamma, y_\gamma)$ is the photon acceptance for a given photon position (x_γ, y_γ) and $F(x_\gamma, y_\gamma)$ is the density of photons at (x_γ, y_γ). The A_γ^* is a good approximation of the true photon acceptance, $A_\gamma \equiv \int\int [F(x_\gamma, y_\gamma) \cdot A_\gamma(x_\gamma, y_\gamma)] dx_\gamma dy_\gamma / \int\int F(x_\gamma, y_\gamma) dx_\gamma dy_\gamma$, only if it is possible to choose such energy interval ΔE_{el} in which $A_{el}(\Delta E_{el})$ is independent on x_γ and y_γ.

However, in reality the $A_{el}(\Delta E_{el})$ depends on the x_γ in each electron energy interval, see Fig. 16. The reason being that the initial electron beam has a sizable angular spread much larger than that expected for the bremsstrahlung electron. Thus this method of controlling the photon acceptance is not credible.

4.4 Energy Scale Correction

The selection and counting the bremsstrahlung candidates is done using the hardwired algorithm and raw (averaged) ADC counts, ADC_γ. Therefore, the registered counting

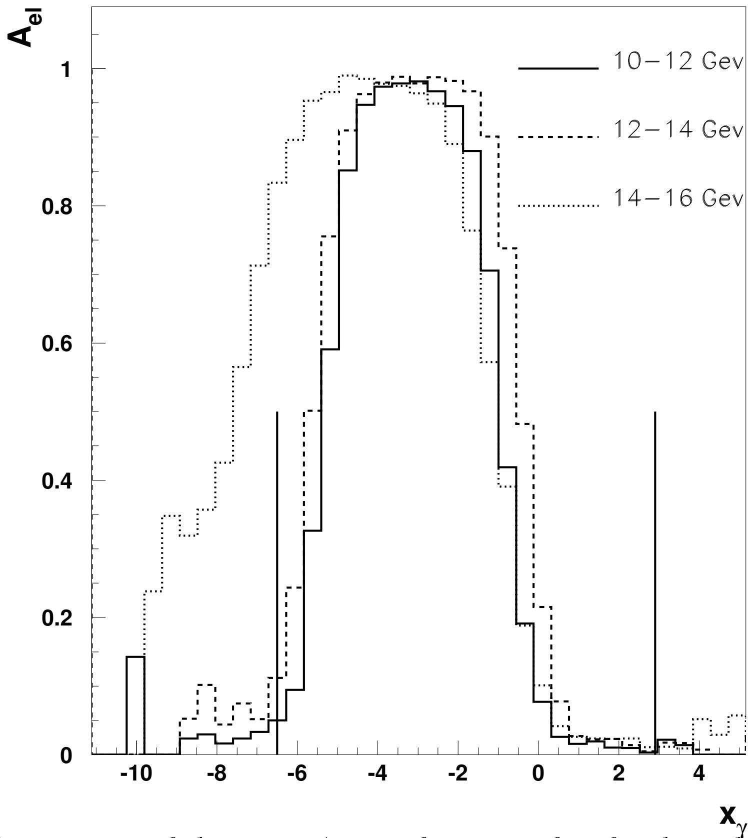

Figure 16: Acceptance of electrons A_{el} as a function of x_γ for three different electron energy intervals.The vesrtical solid lines mark the absolute limits of the geometrical acceptance of photons in x-coordinate.

rates have to be corrected for the overall gain and changing ADC pedestals as well as for the non-linearities and fluctuations in the photon detector response.

From the simulations of the photon detector using the EGS4 program [20] it was found that the average response of the photon detector can be well described above photon energy of 1 GeV by a linear function with a small quadratic non-linear term. Additionally, it was found using the test measurements with the LED pulser that the readout electronics also introduces a relative deviation from linear behavior of about 7×10^{-4} per GeV. Therefore, the average detector response, $\overline{ADC_\gamma}$, could be parametrized as a function of the 'true' photon energy E_γ:

$$\overline{ADC_\gamma} = c_\gamma[1 + f_{nl}(E_e - E_\gamma)](E_\gamma - E_{filter}) + ADC_\gamma^{ped} \tag{11}$$

where c_γ is a conversion constant from GeV to ADC counts (sensitive to the overall gain), f_{nl} is the global non-linearity parameter, and E_{filter} is the parameter accounting for energy loss in the carbon filter. The fluctuation of the response function is modeled by a Gaussian smearing of the energy deposition in the calorimeter due to the sampling fluctuations, $\Delta E/E = \sigma_0/\sqrt{E_\gamma(GeV)}$.

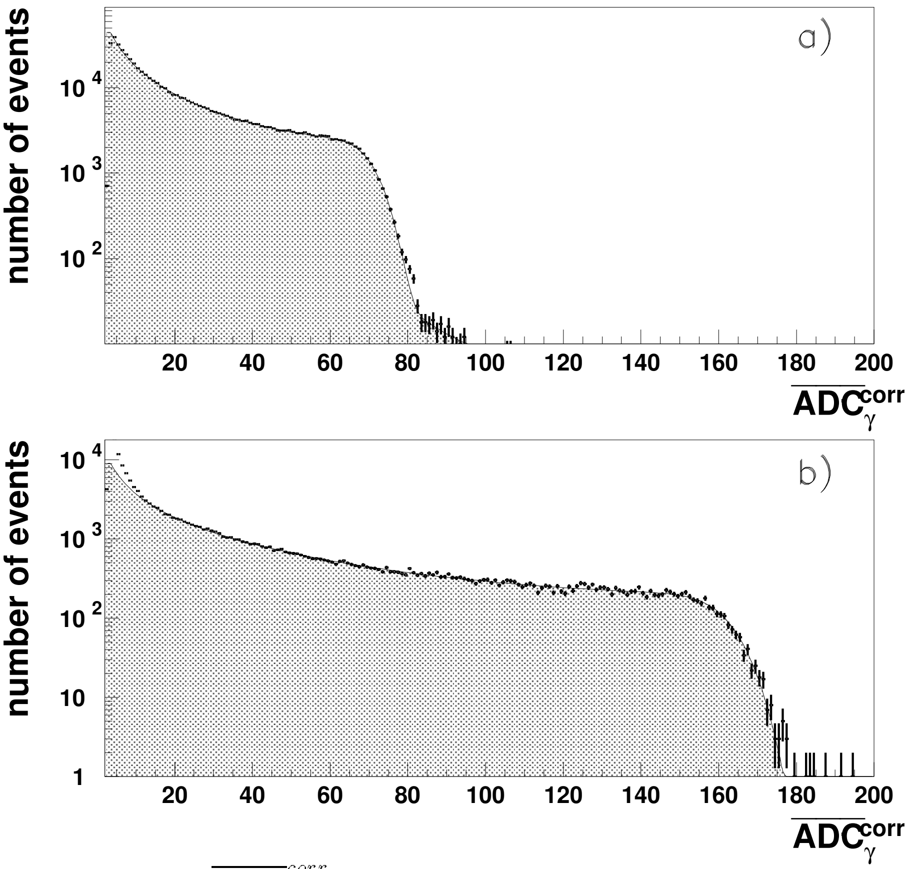

Figure 17: Fit to the $\overline{ADC}_{\gamma}^{corr}$ distributions from the 12 (a) and 27.5 (b) GeV *egas* high statistics runs. The fitted parameters are the normalization factors, one conversion factor c_γ (gain calibration), energy resolution σ_0, E_{filter} and f_{nl}.

The parameters c_γ, f_{nl}, E_{filter} and σ_0 are obtained from the fits to the data. For that purpose dedicated *egas* data were taken when the proton beam was not circulating and the electron beam was stored at two energies of 12 and 27.5 GeV. This ensured low event rates hence no pile-up effects, contribution of only one type of bremsstrahlung and a large lever arm in studing the energy dependencies. Finally, the function, $F_{egas}(ADC_\gamma)$, fitted to the experimental ADC_γ distribution is a convolution of *egas* bremsstrahlung cross section σ_{BH}^{egas} and a function describing Gaussian smearing due to the finite calorimeter energy resolution:

$$F_{egas} = P \int_{0.1\ GeV}^{E_e - M_e} \exp(-\frac{[E_\gamma - \hat{E}_\gamma(ADC_\gamma)]^2}{2{\sigma_0}^2 E_\gamma}) \frac{\mathrm{d}\sigma_{\mathrm{BH}}^{\mathrm{egas}}}{\mathrm{dE}_\gamma} \frac{dE_\gamma}{\sigma_0 \sqrt{E_\gamma}}, \tag{12}$$

(F_{egas} is the function of ADC_γ) where P is the normalization factor, $\hat{E}_\gamma$ is the reconstructed photon energy for given ADC_γ (inverse of Eq. 11). In calculation of σ_{BH}^{egas} the average charge of the gas molecule $Z_A = 4.2$ is assumed but uncertainty due to not exactly known composition of the residual gas is negligible.

In Fig. 17 a simultaneous fit to the data at two beam energies is shown. The distributions of $\overline{ADC}_{\gamma}^{corr}$ are corrected for unequal ADC bins (typically, a bin width differed by 10% from the average). The gain change between two runs of 0.5% is estimated using results of the LED pulse measurements. Six parameters are fitted in the energy range above

≈ 2 GeV: two normalization factors, one conversion factor c_γ providing the overall gain calibration, and three more parameters describing the response of the photon detector, $\sigma_0 = 0.23$, $E_{filter} = 200$ MeV and $f_{nl} = 0.0011$ GeV^{-1}. Quality of the fit is very good and the values of the fitted parameters are in a good agreement with expectations based on the EGS4 detector simulation. In the low energy part (especially for the 27.5 GeV data) of the measured spectrum, which is not included into the fit, a significant contribution from thermal photons Compton scattering can be seen.

In the next step, the Monte Carlo program [7] generates ep bremsstrahlung events using BREMGE [18] and simulates the detector response assuming the nominal values the parameters $\sigma_0, E_{filter}, f_{nl}$ and c_γ. The simulated ADC_γ is used to calculate the observed cross section for each trigger type:

$$\sigma_{BH}^{corr} = \sigma_{BH} N^{sel}/N^{all} \tag{13}$$

where N^{sel} is the number of selected events for each trigger type, σ_{BH} is the total ep bremsstrahlung cross section for the photon energies above 0.1 GeV and N^{all} is the number of all generated events in this energy range.

Once per ZEUS run the calibration constant c_γ is obtained from fits of F_{egas} to the $egas$ data taken concurrently using the electron pilot bunches. The other parameters, σ_0, E_{filter} and f_{nl} are kept constant. The $egas$ data are corrected for the gain variation measured with the help of LED pulser and for changes of pedestals estimated on the basis of the random trigger data. This procedure allows the determination of the actual value of the calibration constant and pedestals in the time intervals (less than 3 minutes). σ_{BH}^{corr} is then corrected for each trigger type by multiplying it by a factor :

$$f = \sigma_{BH}^{actual}/\sigma_{BH}^{nominal} \tag{14}$$

where σ_{BH}^{actual} and $\sigma_{BH}^{nominal}$ are the inegrated theoretical cross sections corresponding to a given trigger type, for actual and nominal values of the calibration constant and pedestals, respectively. It was checked that for not too large variation of the calibration constant ($< \pm 10\%$) and the pedestals ($< \pm 2$ ADC) from their nominal values the factor f obtained that way is very well reproduced by the full MC simulation.

5 Calculation of the Systematic Errors

5.1 Event Pile-up

The error due to this correction (see section 4.1) is of the order of 0.1%. It is estimated by comparing the ratios of the luminosities measured using different triggers as a function of the event rate, see Fig. 18.

For the uncorrected luminosities a clear rate dependence is observed which almost disappears once the correction for the event pile-up is applied. The residual rate dependence of these ratios is taken as a measure of the systematic uncertainty of this correction.

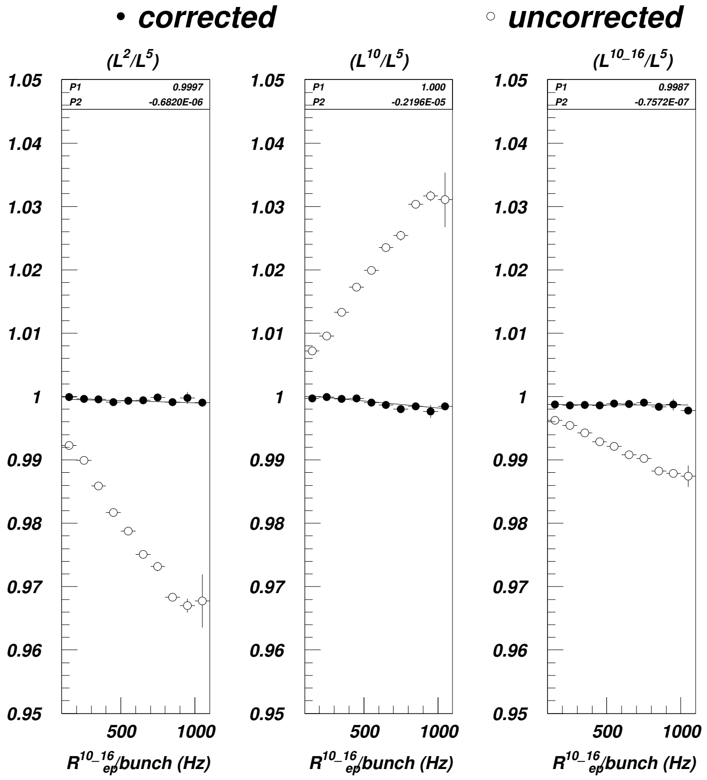

Figure 18: The relative difference between luminosities measured using 2, 10 and $(10-16)$ GeV triggers and the 5 GeV trigger luminosity, as a function of the ep rate, before (open circles) and after (full points) correction for the event pile-up.

5.2 egas Background Subtraction

The assumption in the $egas$ statistical subtraction (see section 4.2) is that the background scales with the electron beam current, and that the factor k is well measured.

To test these assumptions, several test runs were taken when only the electron beam was stored. For these runs the observed rate of bremsstrahlung photons for a given bunch should be proportional to its current, thus the rate divided by the bunch current, R^{BCN}/I^{BCN}, should be BCN independent. Small deviations are however observed. In particular the normalized rates are systematically lower for the leading bunches in a bunch train.

Similar studies are done using the electron pilot bunch data taken in regular running conditions, see Fig. 19.

In both cases, the deviations do not exceed 3% which is taken as a measure of the uncertainty in the estimate of factor k, see Eq. 9. This results in about 0.1% error due to the $egas$ subtraction uncertainty.

5.3 Acceptance Error

The error in the geometrical acceptance determination (see section 4.3) is estimated by:

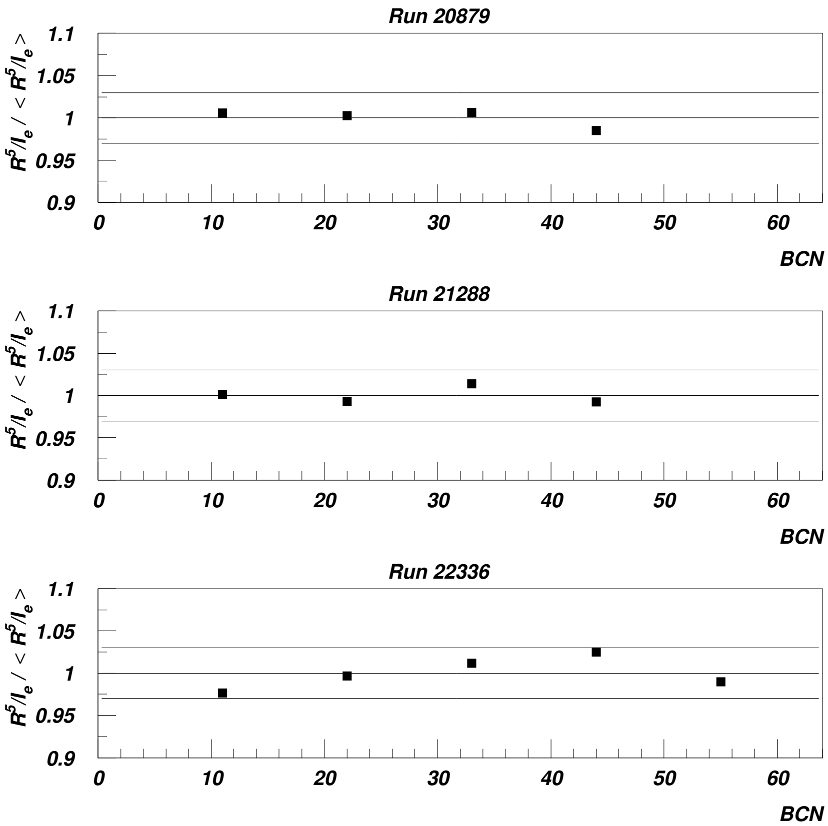

Figure 19: The normalized *egas* rates, R^{BCN}/I^{BCN}, measured in three typical runs using the electron pilot bunches. Solid lines correspond to a 3% deviation from unity.

- varying the shape of the acceptance contour by moving each edge within ± 1 mm as allowed by the calibration data;
- varying the beam divergence by ± 0.01 mrad according to observed typical variations within a single run.

The total A_γ uncertainty is 0.8%.

5.4 Theoretical Cross Section Uncertainty

Calculations at the Born level but taking into account the proton spin, its structure, and the effects of proton recoil [21] or, Z boson exchange [22], agree within 0.3% with Eq. 3. Higher order corrections have been also considered [23], and result in a correction of about -0.2%. The cross-section for the inelastic $ep \to e'\gamma X$ bremsstrahlung has been found to be negligible [24].

The beam size effect for the nominal selection cuts requires -1.92%,-0.83%, -0.29% and -0.53% cross section corrections for $E_\gamma > 2, 5, 10$ GeV and $10 < E_\gamma < 16$ GeV triggers,

Contribution	Trigger			
	2 GeV	5 GeV	10 GeV	$(10-16)$ GeV
calibration constant	0.13%	0.20%	0.32%	0.08%
pedestal	0.16%	0.10%	0.07%	0.07%
ADC bins	0.5%	0.3%	0.2%	0.2%
detector response	0.7%	0.5%	0.5%	0.5%
Total energy scale error	0.75%	0.55%	0.6%	0.5%

Table 1: Systematic errors of the luminosity measurement due to the energy scale uncertainty.

respectively. Uncertainty of these corrections according to Ref. [8] are 0.9%, 0.3%, 0.1% and 0.2%, respectively.

Finally, the total theoretical uncertainty for the four trigger types is estimated to be 1.2%, 0.6%, 0.4% and 0.5%, respectively.

5.5 Energy Scale Errors

The calibration constant uncertainty uncorrelated with the other parameters describing the detector response was estimated by comparing the short time (of the order of few hours) changes of the fitted calibration constant with the variation of the overall gain as measured by the LED pulser (0.3%) and from the MC simulations as difference between the fitted and true calibration constant (0.1%). These two uncertainties were added in quadrature. The contribution to the energy scale error due to the calibration constant uncertainty correlated with the other fit parameters are included in the detector response uncertainty described later.

Uncertainty in pedestal determination is evaluated from the spread of the pedestal values of 0.03 ADC counts, for the colliding bunches, and from the uncertainty in knowledge of the actual position of the ADC bin (FADC non-linearity). This uncertainty affects also the event selection which is estimated by varying in the Monte Carlo simulation the ADC bin widths within allowed ranges.

The systematic error due to the uncartainty in the simulation of the detector response was estimated by repeating the whole procedure described in Sec. 4.4 for different fit ranges, for σ_0 between 0.21 and 0.25 and for a changed intercalibration between the 12 and 27.5 GeV runs. For each set of the fitted parameters new observed cross sections are calculated. The maximum deviation of σ_{BH}^{corr} from the nominal value, for each trigger type, is then used as a measure of the systematic error.

Table 1 summarizes contributions to the energy scale error for different triggers. The total error is obtained by adding all contributions in quadrature.

As a final check of the energy scale understanding the relative difference of the luminosities from different triggers, $\Delta L/L = (L_5 - L_i)/L_5$ is studied. In Fig. 20 $\Delta L/L$ is

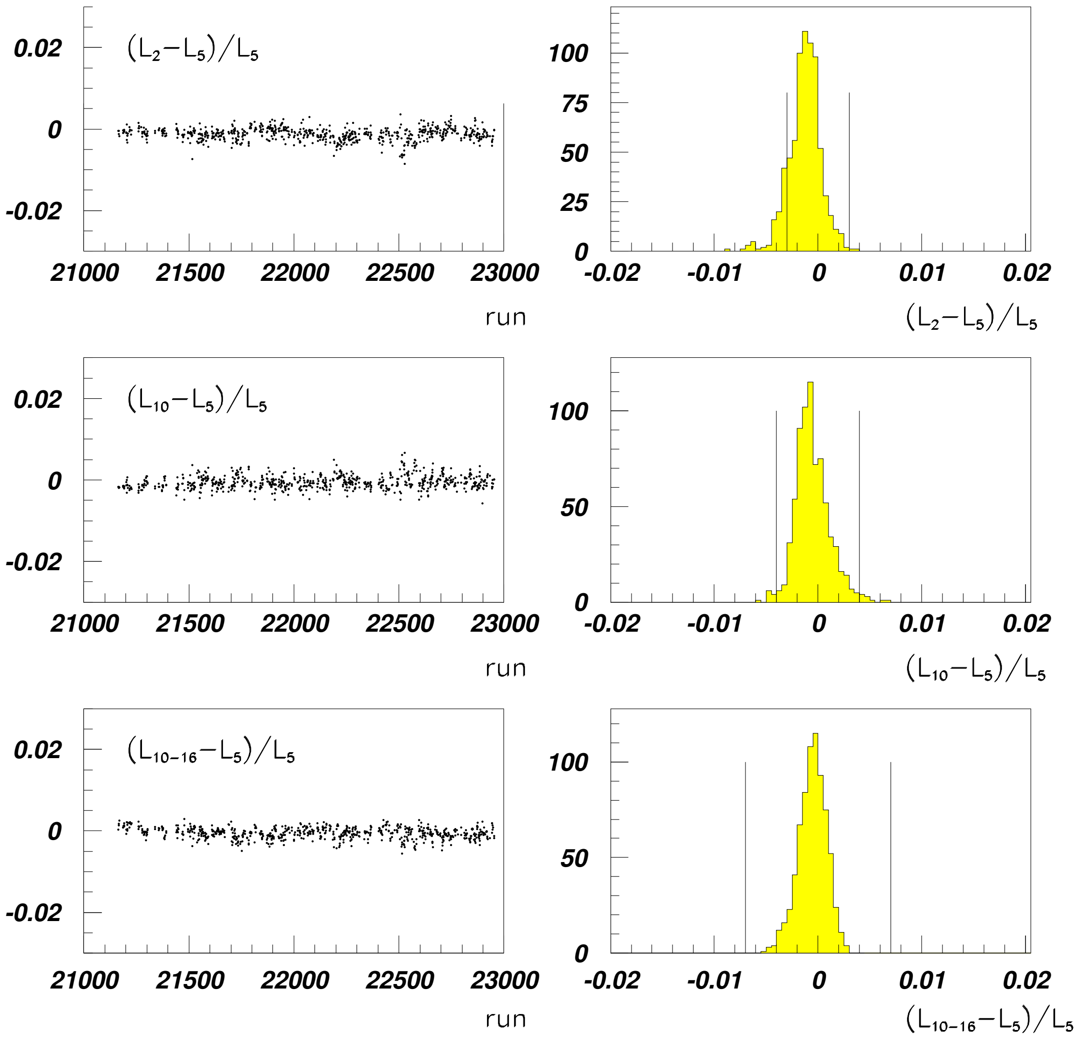

Figure 20: The relative difference between luminosities measured using 2, 10 and $(10-16)$ GeV triggers and the 5 GeV trigger luminosity. The systematic errors calculated for the ratios are represented by vertical lines.

shown as a function of the run number. No significant or systematic deviations are observed. All the observed differences are well contained within systematic errors calculated for these ratios, providing a valuable error cross-check.

The similar study has been performed for the *egas* bremsstrahlung where uncertainties due the beam size effect and the events pile-up are not present. Here also the results confirmed the estimate of the systematic uncertainties due to the energy scale error.

5.6 Total Error

To a good approximation all the discussed uncertainties can be treated as independent and in calculation of the total systematic error can be added in quadrature. In Tab. 2 the summary of the contributing uncertainties to four types of the luminosity measurement are shown. Except for the first method the total error of about 1% is dominated by the acceptance uncertainty. The next significant contributions are due to the energy scale errors and uncertainties in the cross section calculation.

Contribution	Trigger			
	2 GeV	5 GeV	10 GeV	$(10-16)$ GeV
acceptance error	0.8%	0.8%	0.8%	0.8%
cross section calculation	1.2%	0.6%	0.4%	0.5%
egas background subtraction	0.1%	0.1%	0.1%	0.1%
multiple events correction	0.11%	0.01%	0.11%	0.03%
energy scale error	0.75%	0.55%	0.6%	0.5%
Total error	1.4%	1.1%	1.06%	1.05%

Table 2: Systematic errors of the luminosity measurement.

6 Summary and Outlook

The HERA luminosity measurement based on the *ep* bremsstrahlung process proved to be a successful concept. The ZEUS luminosity monitor measuring very forward high energy photons and electrons has been working reliably and allow to achieve a 1% luminosity determination, much beyond initial goal of 5% precision [4]. Nevertheless there is still room for further improvements. Provided better understanding of the photon acceptance and improved understanding of the beam size effect, a sub-percent precision could in principle be achieved. However, the planned HERA upgrade will result in about 5-fold increase in luminosity. Due to much stronger bending of the electron beam close to the IP, the level of synchrotron radiation will also significatly increase. These two factors will require extra effort to maintain the precision of the measurement. Especially, ensuring a good understanding of the detector performance in these difficult conditions will be very challenging.

Along with the luminosity measurement the ZEUS luminosity monitor has other important applications:

- fast online monitoring the HERA performance during the beam steering and the luminosity optimization including measurement of the electron beam angular profile, hence the beam focusing and its trajectory at the IP (beam tilt);
- measurement of the initial state radiation (ISR) in *ep* interactions at HERA;
- tagging of quasi-photoproduction events at HERA.

7 Acknowledgments

The ZEUS Luminosity Group is deeply grateful to the DESY Directorate and the ZEUS experiment management who for over the past 10 years have encouraged, fully supported and advised us in our work. We wish to thank all those people who have not spared their time to advise and discuss with us all our problems. Here, in particular our special thanks are due to R.Klanner, E.Lohrmann and G.Wolf. We wish to thank specially

K.Piotrzkowski whose contribution to the analysis of the luminosity data was large. Many thanks are due to our colleagues who have contributed much work especially in the first stages of design and construction of the luminosity monitor and in particular A.Dwuraźny, K.Eskreys, J.Halik, Z.Jakubowski, B.Machowski and Z.Duliński. We would like to express much gratitude to the HERA machine crew for help, understanding and fruitful collaboration. Without the help of all these people the accomplishment of our work would be impossible.

References

[1] J.Andruszków et al., *First Measurement of HERA Luminosity by ZEUS Lumi Monitor*, DESY 92–066 (1992).

[2] A.A.Sokolov and I.M.Ternov (Moscow State Univ.), Phys. Dokl. **8** (1994) 1203.

[3] D.Kisielewska et al., *Fast Luminosity Monitoring at HERA*, DESY-HERA report 85–25 (1985).

[4] ZEUS Collaboration, *The ZEUS Detector*, Status Report, September 1987, PRC 87–02; Status Report, March 1989.

[5] H.Bethe and W.Heitler, Proc.Roy. Soc., **A146** (1934) 83.

[6] R.L. Glueckstern and M.L.Hull, Phys.Rev., **90** (1953) 1026.

[7] K.Piotrzkowski, Z.Phys., **C67** (1995) 577.

[8] G.L.Kotkin, V.G. Serbo and A.Schiller, Int. J. Mod. Phys., **A7** (1992) 4707; see also references cited there.

[9] M.Derrick et al. (ZEUS Collab.), Zeit. f. Phys. **C69** (1996) 607.

[10] M.W. Krasny, W. Płaczek and H. Spiesberger, Zeit. f. Phys. **C53** (1992) 687.

[11] M.Derrick et al. (ZEUS Collab.), Zeit. f. Phys. **C63** (1994) 391;
Phys. Lett. **B293** (1992) 465.

[12] J. Breitweg et al. (ZEUS Collab.), Zeit. f. Phys. **C75** (1997) 421.

[13] J. Breitweg et al. (ZEUS Collab.), Eur. Phys. J. **C14** (2000) 213¸

[14] A.Kotarba and K.Piotrzkowski, Nucl. Instr. and Meth. **A387** (1997) 235.

[15] The ZEUS Detector, Status Report, ZEUS Collaboration, March 1993.

[16] K.Piotrzkowski, *Experimental Aspects of the Luminosity Measurement in the ZEUS Experiment*, DESY-F35D–93–06, October 1993, Ph.D.Thesis.

[17] L.Suszycki, *Luminosity Monitor for the ZEUS Detector at HERA - The Eye of ZEUS*, Scientific Bulletin of Univ. of Mining and Metallurgy **No 1531**, Physics, Bull.30, Cracow 1993.

[18] K.Piotrzkowski and L.Suszycki, BREMGE, *A Monte Carlo Generator of High Energy Electron-Proton and Electron-Nucleus Bremsstrahlung Event Generator*, Proc. of the Workshop, Physics at HERA, ed. W.Buchmüller and G.Ingelman, Hamburg (1991) 1463.

[19] R. Brun and F. Carminati, CERN Program Library Long Writeup W5013, 1993 (unpublished).

[20] R. L. Ford and W. R. Nelson, SLAC (1978) 210;
W. R. Nelson, H. Hiryama and D. W. Rogers, SLAC (1985) 265.

[21] K.J.F.Gaemers and M.van der Horst, Nucl. Phys. **B316** (1989) 269;
Erratum, ibid. **B336** (1990) 184.

[22] A.A.Akhundov, D.Yu.Bardin and L.V.Kalinovskaya, Zeit. f. Phys. **C51** (1991) 557.

[23] M.van der Horst, Nucl. Phys. **B347** (1990) 149.

[24] M.van der Horst, Phys. Lett. **B244** (1990) 107.